

A combinatorial TRM-OFP module bilaterally fine-tunes tomato fruit shape

Biyao Zhang^{1,2*} , Qiang Li^{2,3*} , Neda Keyhaninejad^{2*} , Nathan Taitano⁴ , Manoj Sapkota⁴ , Ashley Snouffer² and Esther van der Knaap^{2,4,5} 

¹National Genomics Data Center, Chinese Academy of Sciences and China National Center for Bioinformatics, Beijing 100101, China; ²Center for Applied Genetic Technologies, University of Georgia, Athens, GA 30602, USA; ³College of Horticulture, Hebei Agricultural University, Baoding, Hebei 071000, China; ⁴Institute for Plant Breeding, Genetics and Genomics, University of Georgia, Athens, GA 30602, USA; ⁵Department of Horticulture, University of Georgia, Athens, GA 30602, USA

Summary

Author for correspondence:
Esther van der Knaap
Email: vanderkn@uga.edu

Received: 22 November 2022
Accepted: 18 February 2023

New Phytologist (2023) **238**: 2393–2409
doi: 10.1111/nph.18855

Key words: fruit shape, morphology, ovate family proteins, tomato, Tonneau1 recruiting motif.

- The mechanisms that regulate the vast diversity of plant organ shapes such as the fruit remain to be fully elucidated. TONNEAU1 Recruiting Motif proteins (TRMs) have been implicated in the control of organ shapes in a number of plant species, including tomato. However, the role of many of them is unknown. TRMs interact with Ovate Family Proteins (OFPs) via the M8 domain. However, the *in planta* function of the TRM-OFP interaction in regulating shape is unknown.
- We used CRISPR/Cas9 to generate knockout mutants in TRM proteins from different subclades and in-frame mutants within the M8 domain to investigate their roles in organ shape and interactions with OFPs.
- Our findings indicate that TRMs impact organ shape along both the mediolateral and proximo-distal axes of growth. Mutations in *Sltrm3/4* and *Sltrm5* act additively to rescue the elongated fruit phenotype of *ovate/Slofp20* (*o/s*) to a round shape. Contrary, mutations in *Sltrm19* and *Sltrm17/20a* result in fruit elongation and further enhance the obovoid phenotype in the *o/s* mutant.
- This study supports a combinatorial role of the TRM-OFP regulon where OFPs and TRMs expressed throughout development have both redundant and opposing roles in regulating organ shape.

Introduction

Many crop plants display extensive shape variation in their fruits, tubers, roots, leaves, and grains. These varied shapes provide more choices for consumers while also providing the cues for the purpose of the produce. For example, certain shapes of tomato are associated with their use in sauces (elongated and blocky types), slicing (large globe types), or eaten fresh (cherry and grape types). Three plant-specific protein families, TONNEAU1 Recruiting Motif family proteins (TRMs), Ovate Family Proteins (OFPs), and SUNs are proposed to control organ shape variations in both dicots and monocots (Wu *et al.*, 2015; Lazzaro *et al.*, 2018; Snouffer *et al.*, 2020).

TONNEAU1 Recruiting Motif proteins are named after their interactions with TONNEAU1 (TON1), a protein that shares similarities with the human centrosomal protein FOP and is essential for microtubule organization in *Arabidopsis* (Drevensek *et al.*, 2012). The TRMs are required to recruit TON1 to the microtubules and preprophase bands (PPB) in a complex that

also includes a phosphatase 2A which together forms the TTP complex (Azimzadeh *et al.*, 2008; Drevensek *et al.*, 2012; Spinner *et al.*, 2013; Rasmussen & Bellinger, 2018). TONNEAU1 Recruiting Motif proteins are important regulators of rice grain shape (S. Wang *et al.*, 2015; Y. Wang *et al.*, 2015; Zhou *et al.*, 2015), *Arabidopsis* leaf and silique shape (Lee *et al.*, 2006; Drevensek *et al.*, 2012), and tomato and cucumber fruit shape (Wu *et al.*, 2018). Interestingly, these TRMs are phylogenetically clustered in the same subclade containing *Arabidopsis* TRM1–5 and appear to function similarly in manipulating cell division (Wu *et al.*, 2018). Specifically, *Arabidopsis* TRM1 and TRM2, tomato TRM5, and rice and wheat *GW7* promote shape elongation by increasing cell proliferation along proximo-distal (periclinal) axis and decreasing cell number in the mediolateral direction (anticlinal; Lee *et al.*, 2006; S. Wang *et al.*, 2015; Zhou *et al.*, 2015; Wu *et al.*, 2018; Wang *et al.*, 2019). This has led to the hypothesis that the orientation of cell division may be influenced by TRMs.

OVATE is the founding member of the OFP family and controls tomato fruit shape (Liu *et al.*, 2002; Van der Knaap *et al.*, 2002). Another OFP member in tomato, *SIOFP20*, interacts

*These authors contributed equally to this work.

synergistically with *OVATE* in controlling the shape of the fruits (Rodriguez *et al.*, 2013; Wu *et al.*, 2018). Natural variation in cultivated tomato led to the map-based cloning of these genes (Liu *et al.*, 2002; Wu *et al.*, 2018). In addition, other OFP members, such as *CaOFP20* in pepper (Borovsky *et al.*, 2021), *OFP1*, 2, 3, 5 in *Arabidopsis* (Wang *et al.*, 2007, 2011; Zhang *et al.*, 2020), *OFP2*, 8, 19 in rice (Schmitz *et al.*, 2015; Yang *et al.*, 2016, 2018; Zhao *et al.*, 2018), *OFP13* in melon, and *OFP20* in potato (Wu *et al.*, 2018), have also been implicated or demonstrated to regulate organ shape in the respective species. Ovate Family Proteins are proposed to change cell division patterns by controlling the plane of cell division as well as cell expansion (Wang *et al.*, 2011; Wu *et al.*, 2018; Yang *et al.*, 2018; Snouffer *et al.*, 2020). However, the molecular mechanism underlying OFP-related shape regulation is far from clear.

At the protein level, both *OVATE* and *SLOFP20* interact with *SITRM5* and 10 other TRMs as evidenced by yeast-two hybrid studies (Wu *et al.*, 2018). These 11 *OVATE*-interacting TRMs contain the M8 domain and targeted mutagenesis revealed this domain is required for the interaction with the OFP domain of *OVATE* (Wu *et al.*, 2018). Follow-up experiments using a *Nicotiana benthamiana* transient expression system and bimolecular fluorescence complementation showed OFPs and TRMs interact in the leaf epidermal cells as well as in yeast via the OFP and M8 domains. Moreover, the subcellular localization of the TRM-OFP protein complex showed that both were either in the cytosol, the microtubules, or in both locations depending on the specific OFP and TRM that were co-expressed. These findings suggest dynamic interactions between OFPs and TRMs and that the subcellular localization may have a functional role in the shape regulatory mechanism of OFPs and TRMs (Wu *et al.*, 2018). Additionally, a knockout mutation of *SITRM5* in the mutant *ovate/Slofp20 (ols)* background reverts the pear-shaped fruit nearly completely back to round (Wu *et al.*, 2018).

To investigate the role of additional TRMs in regulating fruit shape, we created loss-of-function mutants using CRISPR/Cas9. Furthermore, in an effort to investigate the role of the TRM M8 domain and whether protein interactions with OFPs are required for shape regulation, we created in-frame deletions of this domain in *TRM5* and *TRM3/4* in *planta*. The genetic and histological analysis showed that knockout mutants *Sltrm3/4* and *Sltrm5* of the AtTRM1-5 subclade act additively in rescuing fruit shape in the *ols* mutant background. Contrary, knockout mutants *Sltrm19* and *Sltrm17/20a* resulted in an obovoid fruit shape, which was opposite of the effect on shape with mutations in *SITRM5* and *SITRM3/4*. These data suggest a more complex role for TRM-OFP interactions and that the TRM-OFP regulon is functioning in a combinatorial manner to control fruit shape. In conjunction with the genetic analyses, we investigated the correlation of expression for OFPs and TRMs during floral and fruit development. The expression analyses demonstrated a temporally coordinated pattern during development, implying that the distinct expression profiles are essential for OFP and TRM regulation of organ development. Collectively, our study suggests a complex pathway involving several TRMs and OFPs to fine-tune tomato fruit shape.

Materials and Methods

Sltrms CRISPR line construction

All TRMs mutants were created in a wild relative of cultivated tomato, LA1589 (*Solanum pimpinellifolium* L.), by using the CRISPR/Cas9 system. Tomato transformation, CRISPR/Cas9 vector, and primers used for *SITRM3/4*, *SITRM19*, *SITRM17/20a*, and *SITRM26a* mutant alleles and in-frame M8 domain alleles for *SITRM3/4* and *SITRM5* are described in Supporting Information Table S1. T0 generations of the mutants were backcrossed to wild-type (WT) LA1589 or other transgene-free mutants once or twice to separate alleles and select against *Cas9*. Mutations were confirmed by Sanger sequencing. The Cas9-free homozygous mutants were obtained in the F₂ or F₃ generations and used for further analysis.

Shape attributes

Ovaries, 10 d postanthesis (dpa) fruits, and mature fruits of all genotypes were scanned at 1200, 600, and 600 d postfloral initiation (dpi), respectively. Ovary and fruit shape were measured with IMAGEJ (Abràmoff *et al.*, 2004) and TOMATO ANALYZER 4.0 (Rodriguez *et al.*, 2010), respectively. Values of the shape attributes 'Shape Index', 'Proximal end Angle', 'Obovoid', and 'Width Widest Position' were obtained from the fruit. 'Shape Index' is the ratio of the maximum height length to maximum width of the object. 'Proximal end Angle' is the angle between best-fit lines drawn through the organ perimeter on either side of the proximal endpoint at 10%.

$$\text{Obovoid} = \frac{1}{2} \times \text{scale_ob}(y) \times \left(1 - \frac{w_1}{W} + \frac{w_2}{W}\right).$$

If Obovoid > 0, subtract 0.4. Otherwise, Obovoid is 0 (*W*, maximum width; *y*, the height at which the maximum width occurs; *w*₁, the average width above that height; *w*₂, the average width below that height; and a scaling function *scale_ob*). 'Width Widest Position' is the ratio of the height at which the maximum width occurs to the maximum height. At least three plants were analyzed for each genotype and 8–10 ovaries or fruits were measured per plant. Means from single plants were used for boxplots and analyzed with Duncan's multiple comparison.

Analysis of cell number, cell shape, and cell division number

Ovaries at anthesis were cut longitudinally before fixation with FAA. Ovary staining and cell number and size measurements of the proximal area were done as described previously (Wu *et al.*, 2018). An exponential growth equation was used to quantify cell proliferation based on the implicit assumption that all cells divide synchronously and continuously from the first cell (Sherley *et al.*, 1995). Therefore, the total cell division number in two axes of a tomato ovary was calculated from the total cell number following the formula:

Total cell division number = $\log_2(\text{final cell number})$.

Three to four plants were analyzed for each genotype. Means of five ovaries from each plant were used for Duncan's multiple comparison test.

Transient expression of proteins in *N. benthamiana*

For the tobacco expression studies, the constructs CFP-OVATE, RFP-TRM5, RFP-TRM19, GFP-TRM19, RFP-TRM17/20a, TRM26a-GFP, RFP-TRM26a, GFP-MAP4, GFP-SITRM3/4^{M8}, and GFP-SITRM5^{M8} were constructed similarly as described for OFP20-GFP, OVATE-RFP, OVATE^{D280R}-RFP, GFP-SITRM3/4, and GFP-SITRM5 (Wu *et al.*, 2018). Full-length WT or in-frame M8 mutant cDNAs of *SITRM3/4* and *SITRM5* were cloned into the Gateway entry vector (Invitrogen) and then recombined into binary destination expression vectors pSITE with N-terminal GFP or RFP tags. The *Agrobacterium tumefaciens* strain C58C1 was used for the transient transformations. Tobacco agroinfiltration and confocal microscopy analysis of fluorescence proteins were performed as described previously (Wu *et al.*, 2018). Separate *Agrobacterium* cultures containing different plasmids were resuspended in infiltration buffer containing 10 mM MgCl₂, 10 mM MES, pH 5.7, and 150 mM acetosyringone at pH 5.6 and adjusted to an OD₆₀₀ of 0.2–0.3 for infiltration. A Zeiss LSM 880 confocal scanning microscope was used to detect GFP or RFP fluorescence with 488 or 543 nm wavelength. Around 100 cells were evaluated in independent experiments that express both proteins.

RNA seq data for expression pattern and correlation analysis

RNA sequencing data of the developmental stages from WT tomato were from four experiments. Inflorescence meristem and floral meristem (IM&FM) and 2 dpi data were from SRP192754; 4–16 dpi data were from NCBI SRP090034; anthesis-stage ovary, 10–30 dpa total fruits data were from SRP017242; Dissected carpel, seed and columella data of 2–10 dpa fruits were from SRP218206. All data were mapped with HISAT2 (Kim *et al.*, 2019) and normalized into TPM (transcripts per million). Clusters of Weighted Gene Correlation Network Analysis (WGCNA) were obtained with all expressed genes at all stages in R using WGCNA package (Langfelder & Horvath, 2008). We used the PickSoft-Threshold function to choose the soft thresholding power value, =20, by applying the approximate Scale-free Topology Criterion. We then used the function blockwiseModules with the following parameters to obtain weighted co-expression modules: power = 20, maxBlockSize = 35 000, TOMType = 'signed', networkType = 'signed hybrid', corType = 'Pearson', minModuleSize = 30, and mergeCutHeight = 0.25. GO enrichment analysis was done using TOPGO R package (Alexa & Rahnenfuhrer, 2021). The significantly enriched GO terms were determined after multiple testing correction by the Benjamini and Hochberg FDR estimation (FDR adjusted *P*-value < 0.05). The enriched GO terms for certain clusters were then curated with REVIGO (Supek *et al.*, 2011). The

graphs and figures were generated using GGPLOT2 package in R (Wickham, 2011). Samples were placed either in the floral development group (including 4, 6, 8, 10, 13, and 16 dpi, anthesis) or fruit development group (including 2 dpa-C, 2 dpa-p, 2 dpa-S, 4 dpa-C, 4 dpa-P, 4 dpa-S, 6 dpa-P, 6 dpa-S, 8 dpa-C, 8 dpa-P, 8 dpa-S, 10 dpa-C, 10 dpa-P, 10 dpa-S, 10 dpa, 20 dpa, and 30 dpa) for gene-specific correlation analysis. The following formula was used to calculate correlation coefficient between two genes.

$$\text{Correl}(X, Y) = \frac{\sum(x-\bar{x})(y-\bar{y})}{\sqrt{\sum(x-\bar{x})^2 \sum(y-\bar{y})^2}}$$

Results

SITRM3/4 and *SITRM5* from subclade I function additively to control tomato fruit shape

SITRM3/4 is the closest paralog of the previously described previously; *SITRM5* and both are clustered with the *Arabidopsis* *TRM1* through *TRM5* clade (Wu *et al.*, 2018). Despite the close evolutionary relationship, these two tomato *TRMs* showed distinct expression patterns in tomato floral and fruit development. *SITRM5* was expressed in most of the examined tissues and was the highest during floral development in 4, 6, and 8 dpi flower buds (Fig. S1). Contrary, the highest expression of *SITRM3/4* was observed in the developing seeds and in young flower buds at later time points than *SITRM5*. Compared with *SITRM5*, the effect of a null in *SITRM3/4* has not yet been investigated. Two different mutation events (a 4- and a 16-bp deletion in the third exon) resulted in a likely loss of function of *SITRM3/4* (*t3*) (Fig. S2). The *t3* effect was slightly different in 10 dpa fruits but not significantly different in mature fruits compared with WT (Figs 1, S3). This might be due to the ripening process in *S. pimpinellifolium* fruits, featuring low firmness and a reduced definition of shape of the fruit. Double-mutant lines for *t3* and *Sltrm5* (*t5*) were generated to investigate the genetic interactions. At 10 dpa, the flat fruit shape of the double mutant was enhanced but only significantly for the proximal end angle trait compared with *t3* or *t5* single mutants, which showed that the strongest effect on fruit shape results from *Sltrm5* (Fig. 1a). At the ripe fruit stage, there was no significant difference in the shape of *t5* vs *t3/t5* mutant in the WT background (Fig. 1b).

SITRM3/4 and *SITRM5* proteins are known to interact and co-localize with OFPs in yeast and tobacco expression systems, respectively (Wu *et al.*, 2018). Additionally, *t5* nearly rescues the elongated pear-shaped phenotype of the *ols* mutants (Wu *et al.*, 2018). To further investigate the genetic interactions between these two OFPs and *TRMs*, *t3* and *t5* mutants were crossed into the *ols* background. Similar to what was previously observed with the *t5* single mutant, *t3* partially rescued the elongated fruit shape of *ols* at 10 dpa and mature stages, albeit to a lesser degree than the *ols/t5* triple mutant (Figs 1, S3). The combination of both *t5* and *t3* in the *ols* background appeared to fully restore round fruit

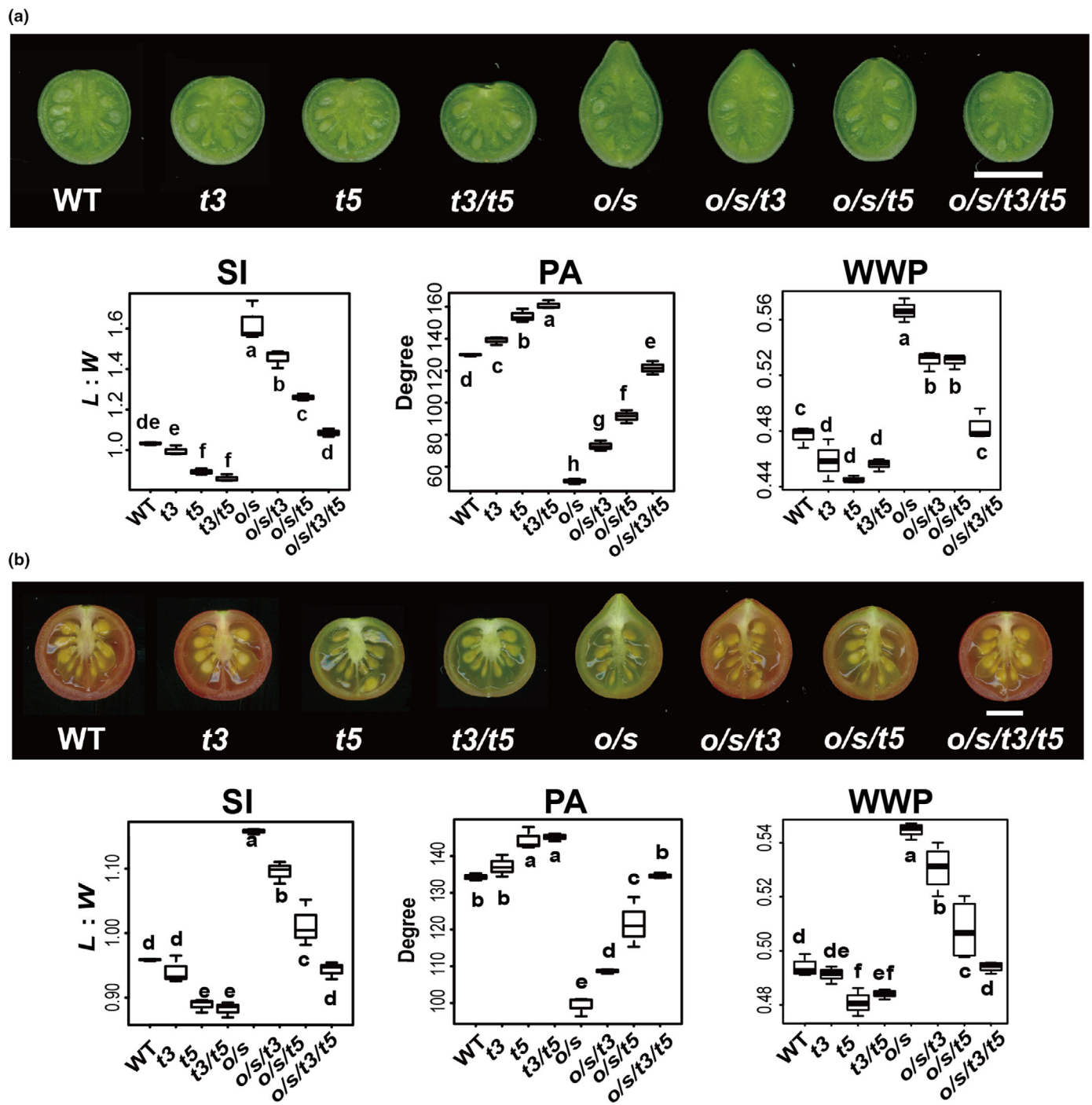


Fig. 1 *SITRM3/4* and *SITRM5* function additively on fruit shape regulation in the *o/s* (*ovate/sov1*) background. (a) Representative 10 d post-anthesis (dpa) fruits and three attributes in wild-type (WT, *Solanum pimpinellifolium*), *Sltrm3/4-1* (*t3*), *Sltrm5-2* (*t5*), and their double mutant. (b) Representative mature fruits and three attributes in the genotypes shown in (a). Bars, 5 mm. L : W, length to width ratio; PA, proximal end angle; SI, shape index; WWP, width widest position. Values are mean \pm SE, and statistical analyses were done with Duncan's test ($\alpha < 0.05$).

shapes as 10 dpa and mature fruits were morphologically indistinguishable from WT in the quadruple mutant (Figs 1, S3).

Together, these data suggest the additive roles of *SITRM3/4* and *SITRM5* in regulating fruit shape but primarily in the *o/s* background. Except for the terminal leaflet, the shape indices in

other organs were significantly decreased in *t5* but had not decreased significantly more in *t3/t5* double mutant in both WT and *o/s* backgrounds (Fig. S4a). In addition to the ovary, the effect of *o/s* was most pronounced in the stamen and cotyledon but in opposite directions (Fig. S4a).

In planta alterations of the M8 domain in *SITRM3/4* and *SITRM5* lead to subtle changes in tomato fruit shape

TONNEAU1 Recruiting Motif protein–OFP interactions are mediated by the M8 domain, found in a subset of the TRMs, and is comprised of 10 conserved amino acids (Wu *et al.*, 2018). Amino acid mutations within the M8 domain in TRMs can reduce or abolish interactions between TRMs and OFPs in yeast and *N. benthamiana* cells (Wu *et al.*, 2018). Similarly, the OFP domain in OVATE and SIOFP20 carries a critical residue, D280 and D265 respectively, that is required for the interaction with the M8-containing TRMs (Wu *et al.*, 2018). While we hypothesize that the M8 domain is functional through its interaction with OVATE and SIOFP20, the *in planta* role of this domain in regulating fruit shape is unknown. We, therefore, engineered a non-functional M8 domain of *SITRM3/4* and *SITRM5* using CRISPR/Cas9 with a single gRNA targeting this domain. Only in-frame deletions were selected with one to three amino acid alterations in the M8 domain. In-frame alleles of *SITRM3/4* (*SITRM3/4*^{M8}) and *SITRM5* (*SITRM5*^{M8}) were obtained, resulting in the loss of a highly conserved valine in *SITRM3/4*, and the loss of the two highly conserved isoleucine and valine and the addition of a positively charged lysine residue in *SITRM5*, respectively (Fig. 2a).

To evaluate the interaction between OVATE and the *SITRM*^{M8} generated by CRISPR/Cas9, the *in planta* M8 mutant alleles were cloned and transiently expressed in *N. benthamiana* leaf epidermal cells (Fig. 2b–h). As expected, the WT and M8 mutant proteins of *SITRM3/4* and *SITRM5* were localized to the microtubules when expressed alone, while WT OVATE and its OFP domain mutant OVATE^{D280R} were in the cytoplasm (Figs 2b, S5). Co-expression of OVATE^{WT} with *SITRM3/4*^{WT} or *SITRM5*^{WT} resulted in TRM relocalization almost exclusively to the cytoplasm (*c.* 94% of the cells), consistent with previous results (Fig. 2c,f; Wu *et al.*, 2018). This relocalization of *SITRM3/4* and *SITRM5* was not due to depolymerized microtubules. When co-expressing MAP4, a microtubule-binding protein, with OVATE^{WT} and *SITRM5*^{WT} using three different fluorescent tags, the microtubular structures were maintained while *SITRM5* and OVATE were predominantly in the cytoplasm similarly as without the co-expression of MBD (Figs 2f, S6). When comparing the relocalization of the *SITRM3/4*^{M8} and *SITRM5*^{M8} when co-expressed with WT OVATE, relocalization of the TRMs was in 4% or 21% of the cells (Fig. 2d,g). The TRM^{M8} relocalization was further reduced when co-expressing these proteins with OVATE^{D280R} (Fig. 2e,h). This result showed that disruption of the interacting domains led to a nearly complete abolishment of the relocalization of *SITRM*^{M8} to the cytoplasm in *N. benthamiana* when co-expressed with OVATE^{D280R}. Therefore, we expect limited interaction of OVATE or SIOFP20 with these TRM M8 mutants *in planta*.

We next evaluated fruit shape in the single *Sltrm3/4*^{M8} (*t3*^{M8}) and *Sltrm5*^{M8} (*t5*^{M8}) and double mutant in WT and *ols* backgrounds (Fig. 2i,j). The *t3*^{M8}, *t5*^{M8} single, and double-mutant *t3*^{M8}/*t5*^{M8} were comparable to WT in fruit shape rather than flattening the organs as seen in the null allele of *t5*. This supported

the notion that the M8 mutations were not nulls. These results also showed that the abolished interaction with OVATE and SIOFP20 did not lead to significantly elongated fruit in the WT background even though a trend was observed in the double *SITRM*^{M8} background. However, the *t3*^{M8}/*t5*^{M8} mutants in the *ols* background appeared to slightly enhance the pear shape of the fruit over that of *ols* (Fig. 2i,j). This finding suggested that these TRMs could interact with other OFPs in addition to OVATE and SIOFP20 in the regulation of fruit shape, or that the interaction with low levels of SIOFP20 (*sov1* is not a null) was further reduced. The elongated shape of the *t3*^{M8}/*t5*^{M8} mutants in the *ols* background was observed in three of four experiments and to variable degrees for each of the shape attributes, suggesting an environmental component to the regulation of shape (Fig. S7). Together, these data support the notion that TRM–OFP interactions are mediated by the M8 domain *in planta* and that mutations in the M8 domain may disrupt protein relocalizations possibly by retaining TRMs at the microtubules in the *ols* background albeit that the effect on fruit shape in these mutants is subtle.

Mutations in certain TRMs from subclade II result in elongated tomato fruit shape

From the yeast-two hybrid studies with OVATE as bait, 11 TRMs were identified and all contain the M8 domain. Collectively, these TRMs fall in multiple subclades (Wu *et al.*, 2018). Two of these subclades carry several OVATE-interacting TRMs: the ArTRM1–5 subclade or subclade I, and the second subclade (II) comprised of *SITRM17/20a* and *b*, *SITRM19*, and *SITRM26a* and *b* (Fig. 3a). The spatial–temporal expression patterns of three subclade II TRMs, *SITRM17/20a*, *SITRM19*, and *SITRM26a* were investigated (Fig. S1a). *SITRM19* was expressed throughout floral and fruit development from the inflorescence meristem to 30 dpa fruit and highly expressed in the seeds and columella of developing fruits with peak expression at 2 dpa (Fig. S1b). *SITRM17/20a* was highest expressed in the pericarp of 6–10 dpa fruit. *SITRM26a* showed consistent expression during ovary and fruit development, with the highest expression in the columella of 2 dpa fruit. The expression patterns of these TRMs implied potentially different roles from *SITRM3/4* and *SITRM5* in fruit shape determination.

To investigate the role of the TRMs in subclade II, mutations in *SITRM19*, *SITRM17/20a*, and *SITRM26a* were generated using CRISPR/Cas9. The gRNA targeting *SITRM19* resulted in a 49-bp deletion (*t19-1*) and a 5-bp deletion (*t19-2*) (Fig. S2). The phenotype of the mutations in *SITRM19* resulted in a more elongated fruit shape in both 10 dpa and mature fruit, with a larger ‘Shape Index’ and ‘Widest Width Position’, and a smaller ‘Proximal Angle’ (Fig. 3b,c). Mutations in subclade II TRMs resulted from a 1-bp insertion and a 2-bp deletion for *SITRM17/20a*, and a 30-bp deletion for *SITRM26a* (Fig. S2). Though the fruit shape of single *Sltrm17/20a* (*t17a*) and *Sltrm26a* (*t26a*) mutants were indistinguishable from WT, the *t17/t19* double mutant produced an enhanced obovoid fruit compared with *t19* alone (Figs 3b,c, S8). Therefore, *SITRM19* and *SITRM17/20a*

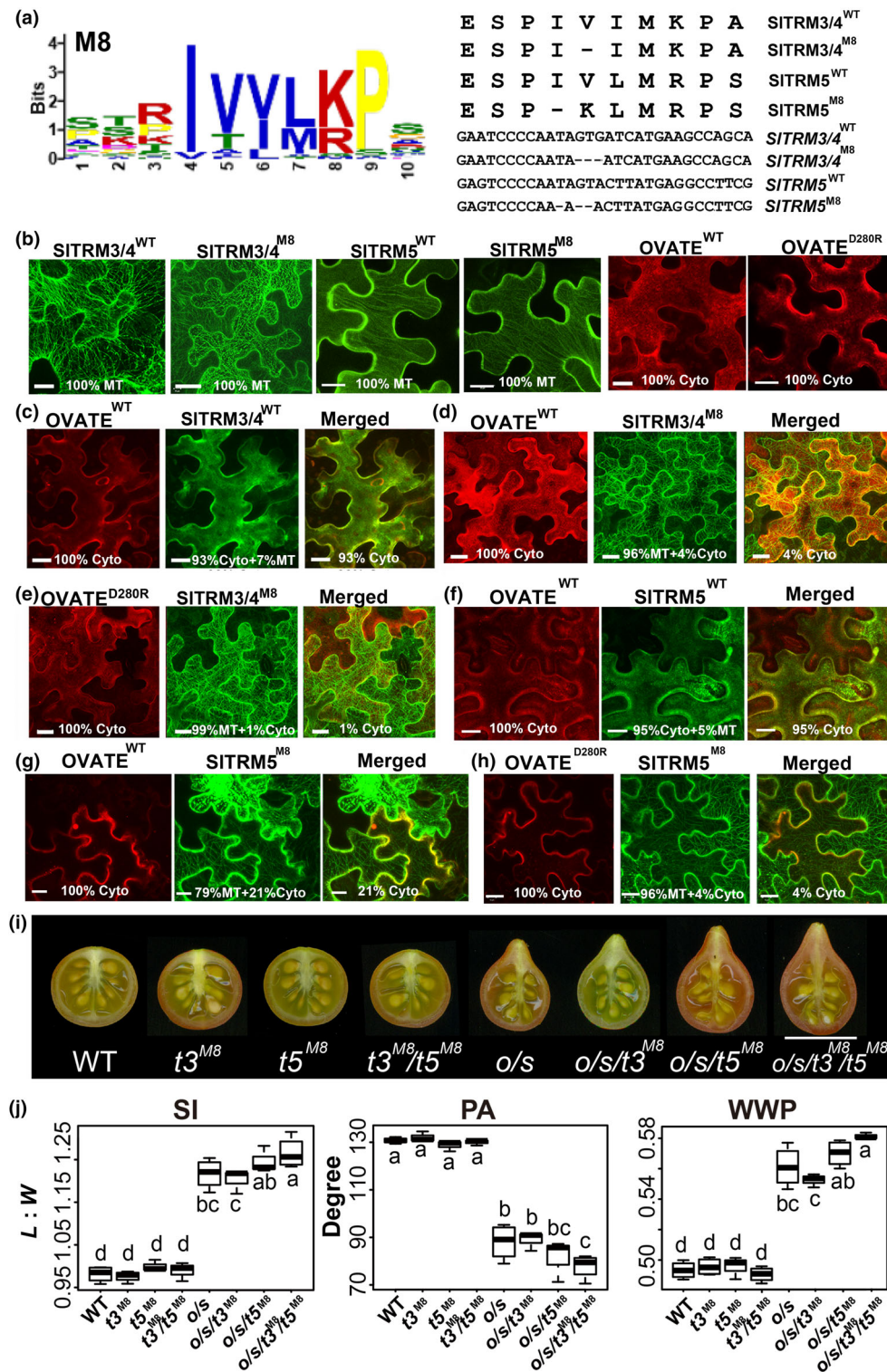


Fig. 2 Ovate Family Proteins (OFP)-TONNEAU1 Recruiting Motif protein (TRM) interactions in M8 domain mutants. (a) CRISPR-Cas9 generated mutations in the M8 domains of SITRM3/4 and SITRM5 in *planta*. Conserved amino acids are shown on the left. Nucleotide mutations and resulting amino acid changes in the mutant M8 alleles of SITRM3/4 and SITRM5 compared with wild-type (WT) are shown on the right. (b) Co-expression of OVATE^{WT} and SITRM3/4^{WT} proteins. (c) Subcellular localization of the individually expressed WT and mutant versions of SITRM5, SITRM3/4, and OVATE in tobacco (*Nicotiana benthamiana*) epidermal cells. (d) Co-expression of OVATE^{WT} and SITRM3/4^{M8}. (e) Co-expression of OVATE^{D280R} and SITRM3/4^{M8}. (f) Co-expression of OVATE^{WT} and SITRM5^{WT}. (g) Co-expression of OVATE^{WT} and SITRM5^{M8}. (h) Co-expression of OVATE^{D280R} and SITRM5^{M8}. Numbers in (b–h) show the proportions of the cells that express both proteins and their subcellular localization. Cyto, cytoplasm; MT, microtubules. (i) Mature fruits of the single or double-mutant SITRM3/4^{M8} and SITRM5^{M8} in the WT or *o/s* (*ovate/sov1*) background. (j) Shape attributes of all genotypes shown in (i). *L* : *W*, length to width ratio; SI, shape index; PA, proximal end angle; WWP, widest width position. Bars: (tobacco cells) 20 μ m; (fruit) 1 cm. Values are mean \pm SE, and statistical analyses were performed with Duncan's test ($\alpha < 0.05$).

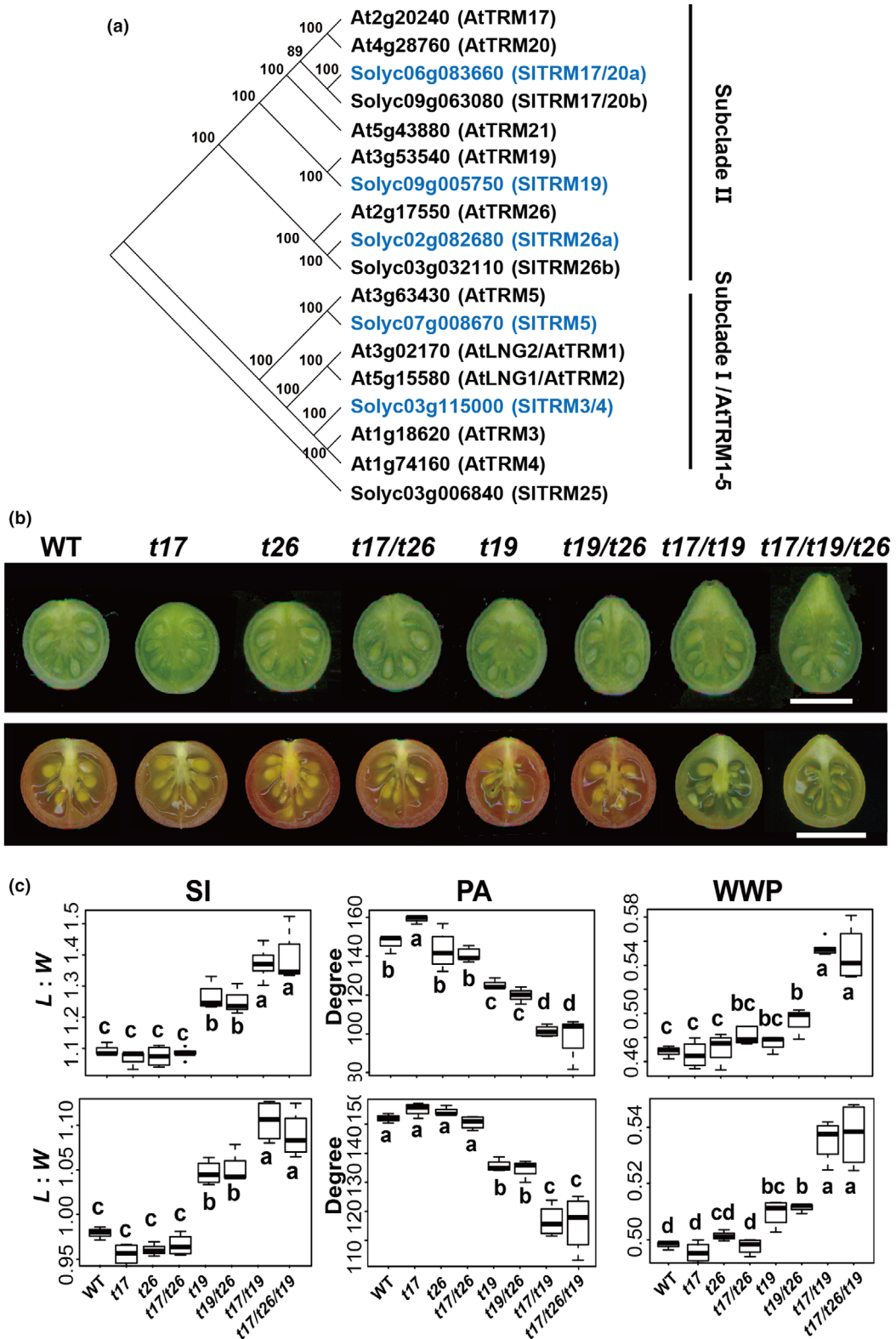


Fig. 3 Functional analyses of TONNEAU1 Recruiting Motif proteins (*TRMs*) from subclade II. (a) A partial phylogenetic tree of the *TRMs* in Arabidopsis and tomato (*Solanum lycopersicum*) using *SITRM25* as the outgroup. In blue are the *SITRMs* from this study. The number at the nodes indicates bootstrap values after 100 permutations. (b) Representative samples of 10 dpa and mature fruit of the single, double and triple mutants of *Sitrm17/20a-1* (*t17a*), *Sitrm26a* (*t26*), and *Sitrm19-1* (*t19*). (c) Shape attributes of 10 dpa (upper panels) and mature fruit (lower panels) in the genotypes shown in (b). *L : W*, length to width ratio; *SI*, shape index; *PA*, proximal end angle; *WWP*, widest width position. Bars: (10 dpa fruits) 5 mm; (mature fruits) 1 cm. Values are mean \pm SE, and statistical analyses were performed using Duncan's test ($\alpha < 0.05$).

show a synergistic effect on fruit shape while the *t26a* mutation had no effect on fruit shape. From this, we conclude that the subclade II TRMs effect shape in an opposite manner of *SITRM3/4* and *SITRM5*.

To genetically test whether the TRMs from the two subclades have an opposing effect on shape, we generated double mutants of *SITRM19* from subclade II and *SITRM5* from subclade I. The double-mutant *t5/t19* was similar to WT as the mutations counterbalanced each other in the 10 dpa and mature fruits (Figs 4a, S9). In the *ols* background, the *t5/t19* mutants partially counteracted each other albeit that the effect of *t5* was stronger than *t19*. Furthermore, comparisons between the combination of heterozygous and homozygous mutations for *t5* and *t19* suggested that the regulation on shape by *t5* and *t19* is impacted in a dose-dependent manner (Fig. 4b). In sum, *SITRM5* and *SITRM19* have an opposing effect on fruit shape in both WT and *ols* backgrounds.

Histological analysis of mature ovaries in wild-type, *trm*, and *ofp* mutants

The effect on fruit shape by *OVATE*, *SIOFP20*, and *SITRM5* is established during floral development (Wu *et al.*, 2018). To determine whether *SITRM3/4* also functions before anthesis to affect final fruit shape, we investigated the ovary shapes of the *trm* mutants in WT and *ols* backgrounds (Fig. S10). The *t3* mutation alone did not affect ovary shape in the WT background, while it did in the *ols* background (Fig. S10a). The shape differences were mainly driven by changes in ovary length and not width.

To investigate the histological basis of altered ovary shape, cell number and cell shape were investigated in the proximal region of the ovaries that showed the clearest impact on organ shape (Fig. 5a,b). In the WT background, the length and shape index of the proximal area was not significantly affected by *t3* and/or *t5*. The width was significantly wider in *t5* mutants compared with WT due to more cells in the mediolateral direction (n^{ml}) of the ovary. In the *ols* background, the length and shape indices were significantly reduced in *t3* and/or *t5*. Contrary to WT, the reduction in the elongated shape for *ols* mutants was driven by the reduced cell number in the proximo-distal direction (n^{pd}). Furthermore, the combination of *t3* and *t5* was additive in restoring the phenotype to WT in the *ols* background.

Changes in organ shape can be driven by the shape of the cells. The ovary cell shapes of the *trm* mutants were highly variable and not consistent in the different genetic backgrounds, suggesting no distinguishable role for cell shape in establishing ovary shape by the TRMs (Fig. S11). Combined, these data implied that the regulation of cell number in the proximo-distal and/or mediolateral direction in the proximal area of the ovary was the major driver in determining organ shape by the TRM-OFP module.

To model the resulting changes in cell division patterning, the total cell number count in an ovary from an initial cell was used to estimate the number of cell divisions and the orientation of those cell divisions. These calculations assume that all cells divide synchronously and continuously within the ovary throughout

development, although that has not been tested within developing ovaries of LA1589 tomatoes. From the total cell number, this calculation suggested approximately nine continuous cell divisions in both WT and the mutants irrespective of the division plane (Fig. 5c). When considering cell division planes, three divisions in the periclinal direction and six in the anticlinal were estimated for WT as well as the single and double *t3/t5*. On the contrary, in the *ols* mutant, approximately four periclinal and five anticlinal divisions occurred, and this effect was partially restored in *t3/t5*. This model suggests that *SITRM3/4* and *SITRM5* function to counter the effect of *OVATE* and *SIOFP20* in organ shape primarily through orientating cell division patterns. Even though mature fruit shape was restored to WT by *t3/t5* in the *ols* background, neither tissue nor cell division patterning in *ols* was fully restored to WT in the ovary, suggesting the presence of other genes working in conjunction with the two TRMs in regulating ovary shape.

With respect to subclade II TRMs, the ovary shape was elongated in *t19* and increased further in *t17/t19* (Fig. S10b). The larger length and shorter width of the ovary in both *t19* and/or *t17/t19* mutants resulted from the increased cell number in the proximo-distal direction and decreased cell number in the mediolateral direction (Fig. 6a). Meanwhile in the *ols* background, *t19* showed an increased length of the proximal area resulting from an increase in cell number in the proximo-distal direction (Fig. 6b). No reproducible effects on cell shape were observed for the subclade II TRM mutants, similar to *t3* and *t5* (Fig. S11b,c). By using the same calculation as for *t3* and *t5*, the *t17/t19* double mutant increased in periclinal and decreased the anticlinal divisions enhancing the effect of *ols* (Fig. 6c). Taken together, these data suggest that *SITRM19* and *SITRM17/20a* function together with *OVATE* and *SIOFP20* in cell division patterning to regulate elongated organ shape and in an opposing manner to *SITRM3/4* and *SITRM5*.

Subcellular relocalization of subclade II SITRMs and SIOFPs

Co-expression of *OVATE* or *SIOFP20* with subclade I TRMs, *SITRM5*, and *SITRM3/4* results in relocalization of the proteins (Fig. 2; Wu *et al.*, 2018). To explore whether protein interaction of clade II TRMs with *OVATE* and/or *SIOFP20* occur as well, we co-expressed the proteins in *N. benthamiana* leaf epidermal cells. When singly expressed, *SITRM19* and *SITRM26a* were detected on the microtubules, whereas *SITRM17/20a* was located in the cytosol (Fig. 7a). When co-expressed with *OVATE*, *SITRM19* had re-localized to the cytosol. When co-expressed with *SIOFP20*, *SITRM19* remained primarily on the microtubules, similar to *SITRM5* (Fig. 7b,c). When co-expressed with *SIOFP20*, *SITRM17/20a* remained in the cytosol, whereas *SIOFP20* was found in the nucleus in fewer cells than when expressed alone (Fig. 7d). When co-expressed with *OVATE* or *SIOFP20*, *SITRM26a* was predominantly relocalized to the cytosol (Fig. 7e,f), similar to *SITRM3/4*. Thus, we conclude that both subclades of SITRMs re-localize when co-expressed with *OVATE* and *SIOFP20*.

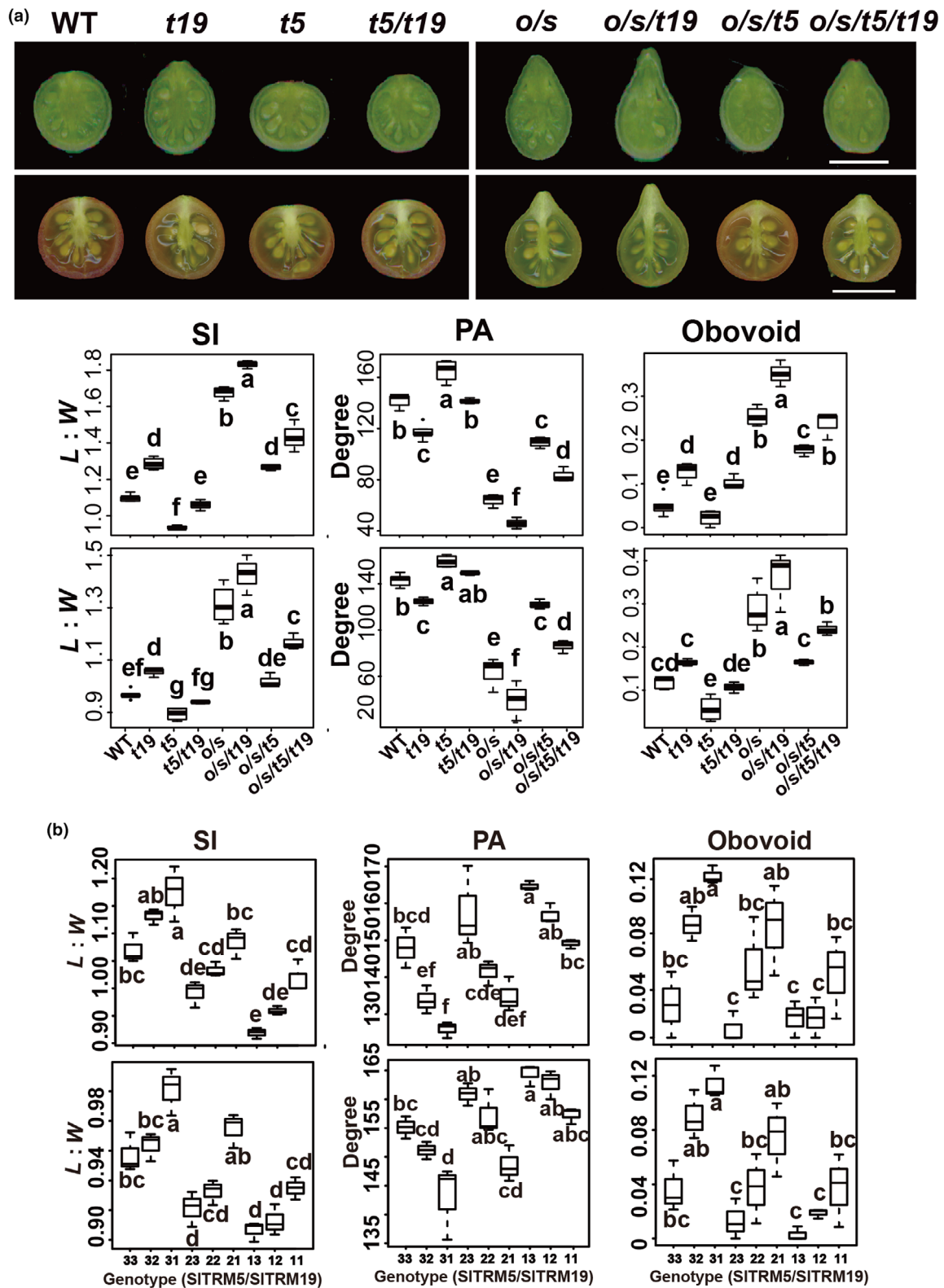


Fig. 4 *Sltrm5* (*t5*) and *Sltrm19* (*t19*) mutually suppress each other in a dose-dependent manner. (a) Ten day post-anthesis (dpa) and mature tomato (*Solanum pimpinellifolium*) fruits of *t5-1*, *t19-1*, and their double mutant in the wild-type (WT) and *o/s* (*ovate/sov1*) background. Bars: (10 dpa) 5 mm; (mature fruit) 1 cm. Measurements of three shape attributes, shape index (SI), proximal end angle (PA), and Obovoid for 10 dpa (upper panels) and mature fruit (lower panels). *L* : *W*, length and width ratio. (b) Dosage effect of the *t5-1* and *t19-1*. The numbers 1, 2, and 3 represent the homozygous mutant, heterozygous, and WT, respectively. Values are mean \pm SE, and statistical analyses were performed with Duncan's test ($\alpha < 0.05$).

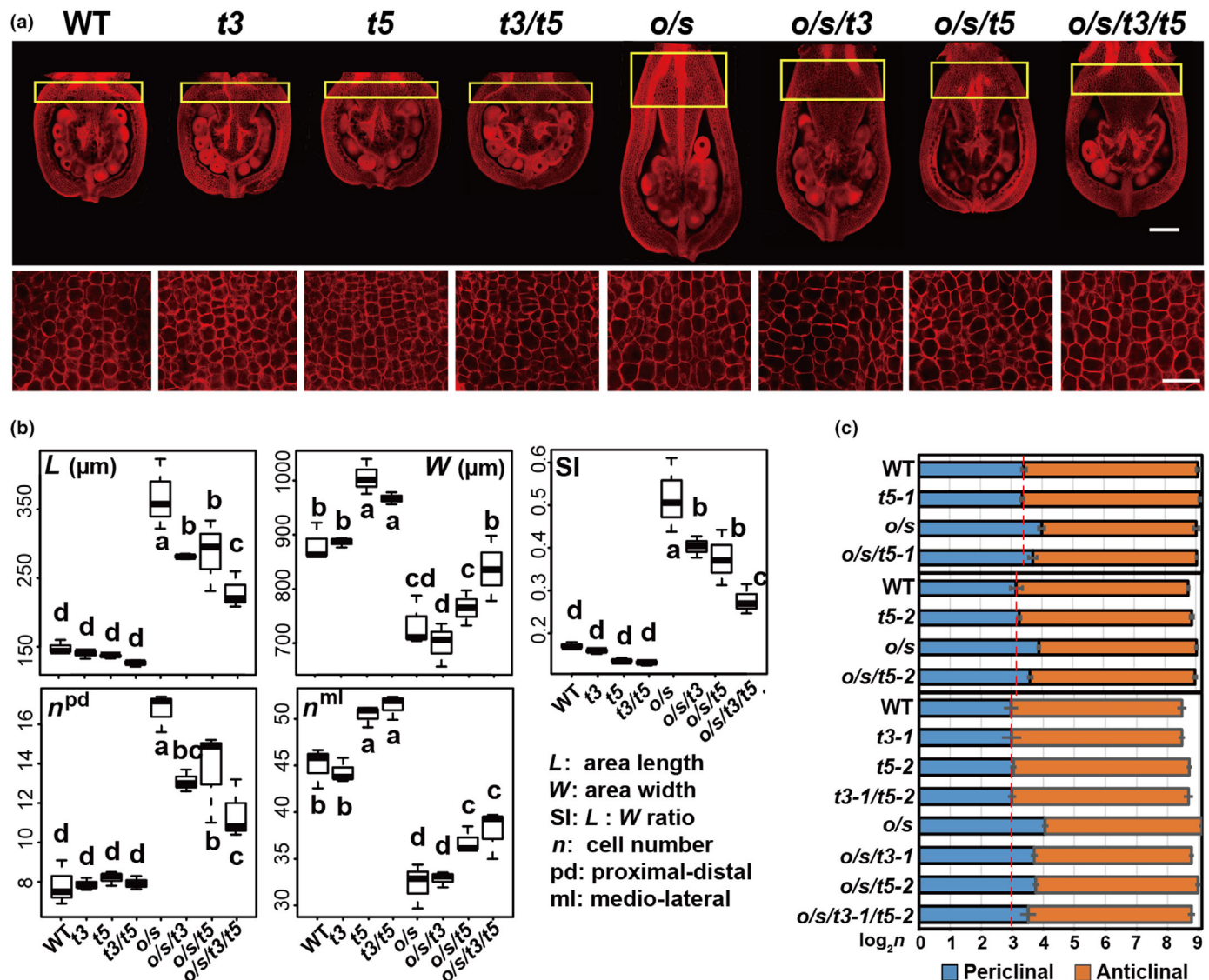


Fig. 5 *SITRM3/4* and *SITRM5* modulate cell number and division orientation in the ovary. (a) Dissected ovaries and cell sections of *t3-1* (*Sitrm3/4*), *t5-2* (*Sitrm5-2*), and their double mutant in the wild-type (WT) tomato (*Solanum pimpinellifolium*) and *o/s* (*ovate/sov1*) background. Boxed region highlights the proximal end areas of propidium iodide-stained ovaries for each genotype. Scale bars represent 200 and 50 μm in the ovary and cell section, respectively. (b) Area length (*L*), width (*W*), and cell number in the proximal end of the ovary in the genotypes in the proximo-distal direction (n^{pd}) or medio-lateral direction (n^{ml}). *SI*, shape index. (c) Calculated cell division frequency in the anticlinal and periclinal direction of *t3* and *t5* in the WT and *o/s* background. Data were collected from three independent experiments. Bars: (ovary sections) 200 μm ; (cell sections) 50 μm . Values are mean \pm SE, and statistical analyses were performed with Duncan's test ($\alpha < 0.05$).

Expression correlation analyses of *TRM-OPF* module

The gene expression patterns for *OPFs* and *TRMs* were temporally and spatially regulated, and are distinct throughout development (Fig. S1). In floral development, *OVATE* and *SITRM5* expression peaked early in the IM/FM meristems and young floral buds, while *SIOFP20* expression peaked much later, namely at anthesis. The other *TRMs* from this study were more highly expressed in developing fruit and/or in a tissue-specific manner. To explore potential molecular functions of the selected *OPFs* and *TRMs*, a WGCNA was performed by combining RNA expression datasets obtained from different stages of floral and fruit development (Fig. 8a). The WGCNA reflected the specific spatial-

temporal expression by grouping these *OPFs* and *TRMs* in clusters of co-expressed genes based on developmental timing and tissue they were expressed in. *SITRM19* and *SITRM26a* were the only genes to cluster together in the WGCNA. GO terms were generated from the correlated gene groups for each cluster containing an *OPF* or *TRM* (Table S2). However, *SITRM3/4* did not have a single GO term that was enriched.

The GO terms that were enriched in the *SITRM5* (light green) cluster of the WGCNA were related to microtubule-based movement and processes, cell division, and the regulation of cell cycle, movement of subcellular components, chromosome organization, and DNA replication. This enrichment was shared with the WGCNA cluster containing *SITRM19/SITRM26a* (blue),

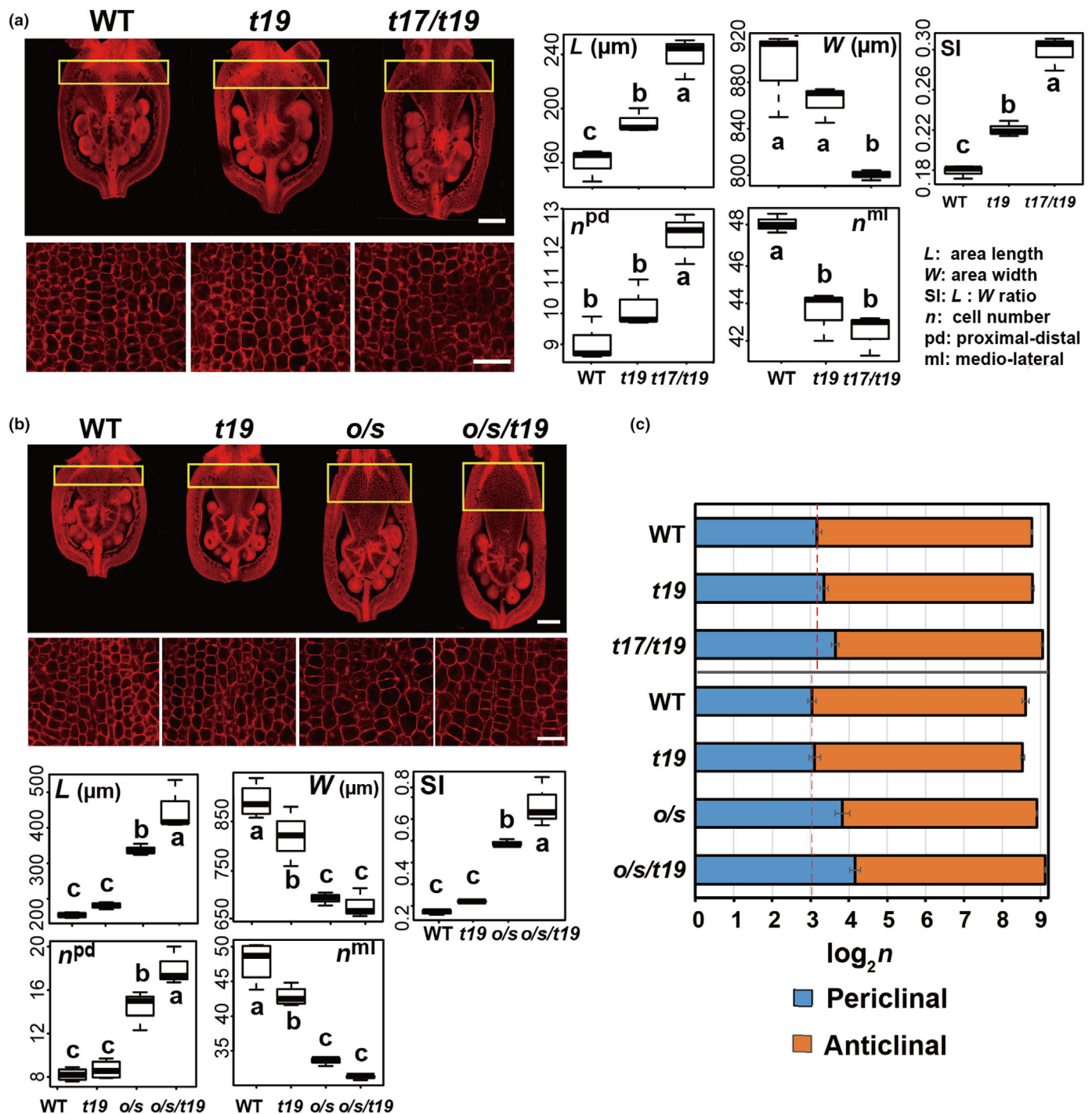


Fig. 6 *SITRM17/20a* and *SITRM19* modulate cell number and division orientation in the ovary. (a) Dissected ovaries and cell sections of *t19-1* (*Sitrm19*) and *t17a-1/t19-1* (*Sitrm17/20a/Sitrm19*) in the wild-type (WT) tomato (*Solanum pimpinellifolium*) background (left), and cell length, width, and cell number in the proximal end of the ovary in the genotypes (right). (b) Dissected ovaries and cell sections of WT, *t19-1*, *o/s* (*ovate/sov1*), and *o/s/t19-1* (upper panels), and cell length (*L*), width (*W*), and cell number in the proximal end of the ovary in the genotypes (lower panels) in the proximo-distal direction (n^{pd}) or medio-lateral direction (n^{ml}). SI, shape index. (c) Calculated cell division frequency in the anticlinal and periclinal direction of all genotypes in two independent experiments. Bars: (ovary sections) 200 μm ; (cell sections) 50 μm . Values are mean \pm SE, and statistical analyses were performed with Duncan's test ($\alpha < 0.05$).

suggesting that these TRMs may have a role in regulating cytoskeleton architecture and cell division throughout development (Table S2). One of the most significant GO terms for the

OVATE cluster (yellow) was regulation of gene expression, shared with the *SITRM19/SITRM26a* cluster, and several cellular biosynthesis processes, some of which were shared with *SITRM5*

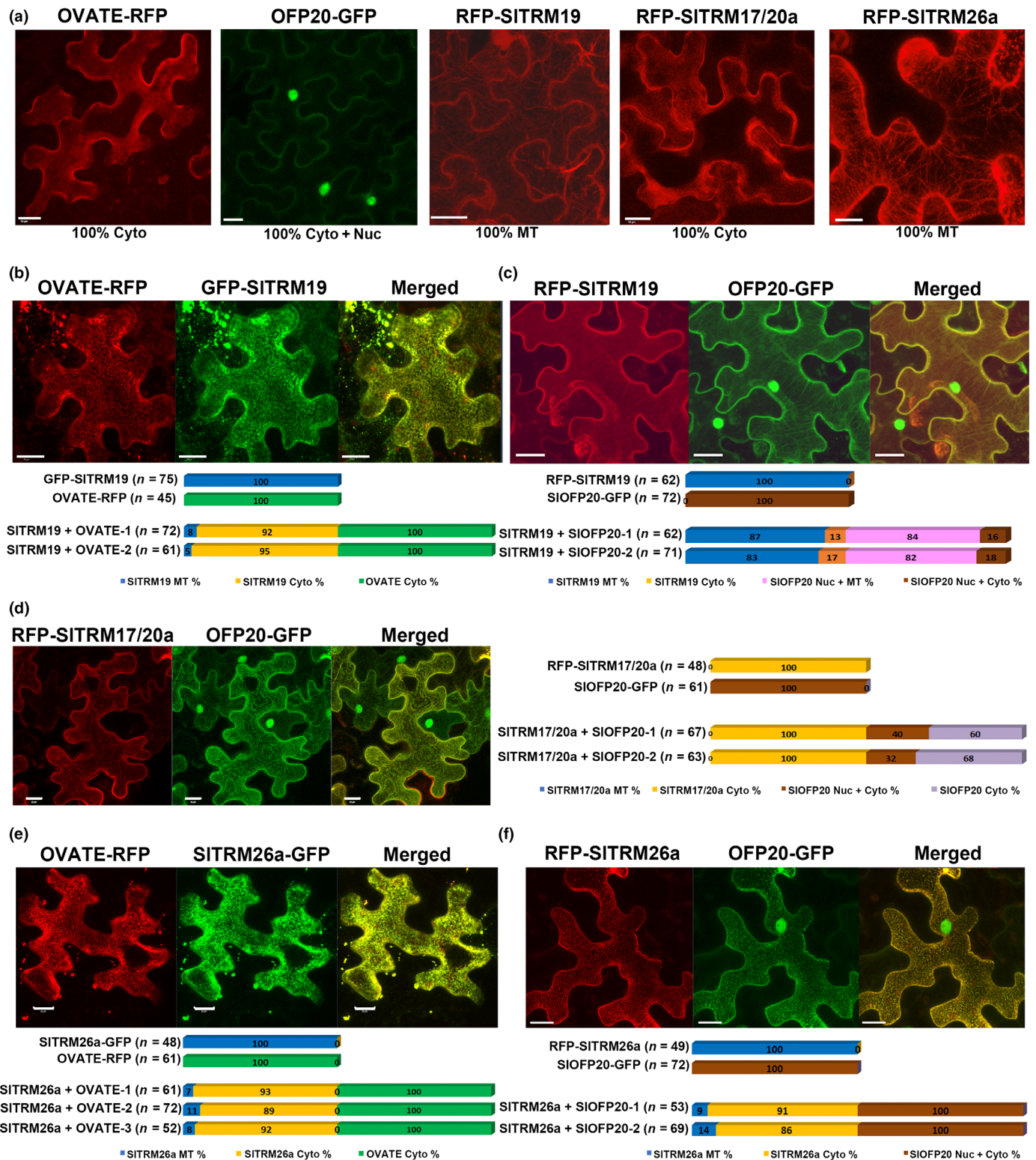


Fig. 7 Co-expression analyses of subclade II SITRMs and SIOFPs in *Nicotiana benthamiana* leaf epidermal cells. (a) Subcellular localization of OVATE and SIOFP20 and subclade II SITRMs when expressed alone. (b) Co-expression of SITRM19 with OVATE. (c) Co-expression with SIOFP20. (d) Co-expression of SITRM17/20a with SIOFP20. (e) Co-expression of SITRM26a with OVATE. (f) Co-expression of SITRM26a with SIOFP20 (f). Bars, 20 μ m. *n*, number of cells expressing both proteins. Cell counts showing percentage of cells with different subcellular localizations were done in two or three biological replicates. Cyto, cytoplasm; GFP, green fluorescent protein; MT, microtubules; Nuc, nucleus; RFP, red fluorescent protein.

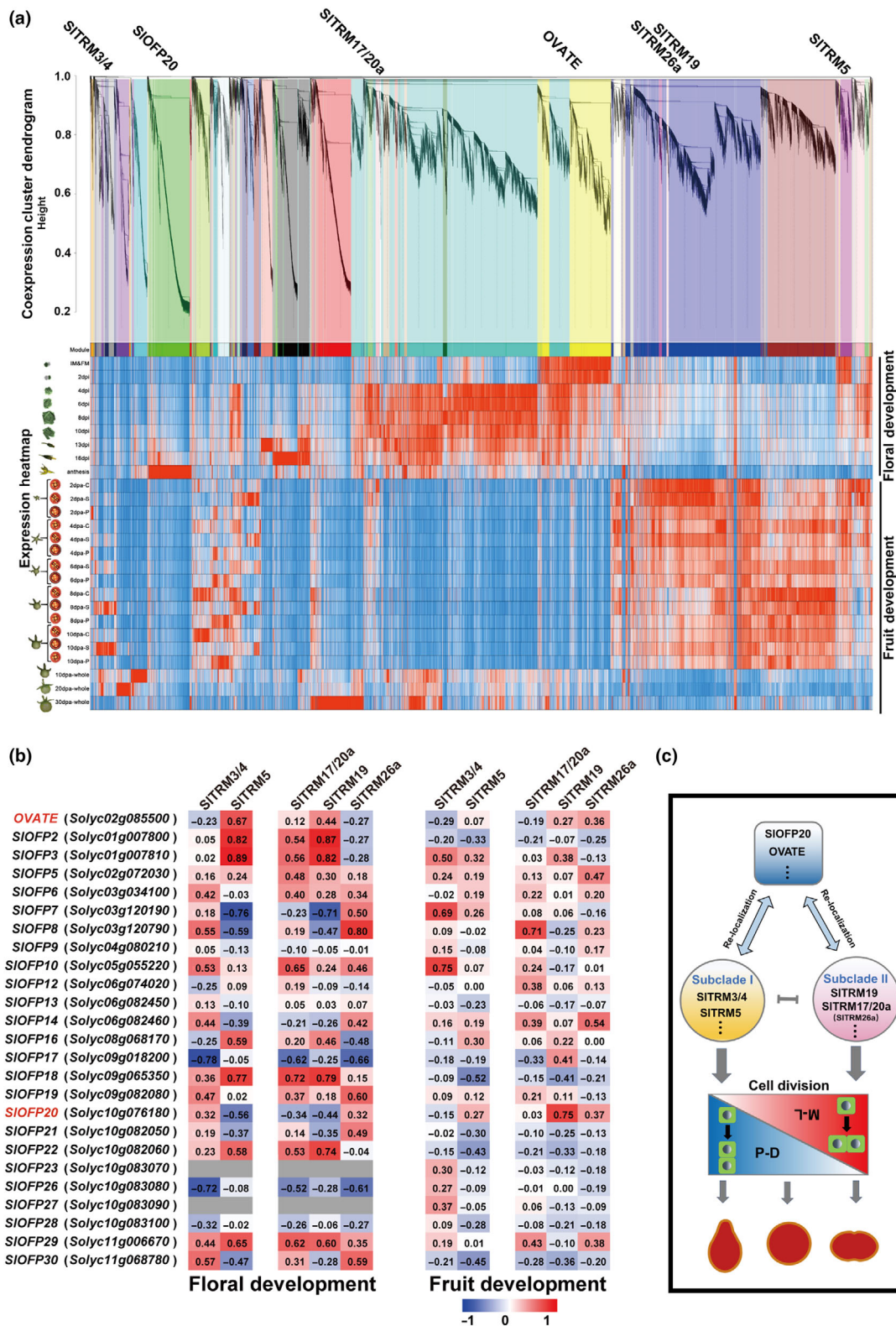


Fig. 8 Co-expression analysis of *SITRMs* and *SIOFPs* during flower and fruit development. (a) Weighted Gene Correlation Network Analysis (WGCNA) during floral and fruit development. Co-expression cluster dendrogram and expression heatmap are shown. C, columella; dpa, days post anthesis; dpi, days past floral initiation; IM&FM, inflorescence meristem and floral meristem; P, pericarp; S, seed; whole, whole ovary. (b) The correlation analyses of two subclade *SITRMs* with all *SIOFPs*. The correlation coefficient between two genes is shown in each box. Values above 0.6 were considered as highly correlation. The red color indicates positive correlations whereas blue color indicates negative correlations. (c) Schematic representation of the TRM-OFP module in fruit shape regulation. The two subclade *SITRMs* appear to manipulate cell division orientation in opposite directions to fine-tune the fruit shape in tomato (*Solanum pimpinellifolium*). OFPs and TRMs dynamically and reversibly interact (double arrowhead) to impact cell division planes (single arrowhead).

(Table S2). *SIOFP20*, within the green cluster of the WGCNA, had significantly enriched GO terms related to growth, cell wall organization, and carbohydrate metabolism which it shared with the *SITRM19/SITRM26a* and the *SITRM17/20a* (light cyan) cluster, respectively. The GO terms enriched for *SITRM17/20a* were related in general to different biosynthetic processes. This was similar for the *OVATE*-enriched GO terms even though the same terms did not overlap. Combined, the GO term enrichment results suggest that the TRM-OFP interaction is multifaceted and impacts the regulation of cell division, cell wall composition as well as microtubule architecture and cell metabolism.

Since the WGCNA clustering did not show much overlap among the *TRMs*, *OVATE*, and *SIOFP20*, we also used the RNA-Seq dataset to evaluate the co-expression of the *TRMs* in this study with the *OFPs* that were expressed during floral and fruit development (Fig. 8b). Co-expressed genes may have roles in similar developmental processes and can be more likely to have a shared biological function (Stuart *et al.*, 2003; Serin *et al.*, 2016). In general, the number of positive correlations between *OVATE* or *SIOFP20* with the *SITRM*s was much higher during floral development than fruit development. *SITRM5* expression in floral development was highly correlated with five *OFPs* (above 0.6) including *OVATE*, while in fruit development, *SITRM3/4* showed the highest correlation with two *OFPs* (*SIOFP7* and *SIOFP10*) (Fig. 8b). Despite the highest expression for *SITRM17/20a* and *SITRM19* in developing fruit tissues, these genes were correlated with two to five *OFPs*, respectively, but only during floral development. Interestingly, during floral development, *SITRM5* and *SITRM19* shared the four most correlated *OFPs* suggesting a mechanism into their counteracting roles in ovary shape (Figs 4, 8b). The correlation of multiple *OFPs* and *TRMs* during development suggests these proteins are part of an intricate interacting network that regulates organ shape.

Discussion

The intricate integration of overlapping mechanisms to regulate plant organ shape is essential to ensure robust organ production within a species under a variety of environmental conditions. Furthermore, the manipulation of one such contributing mechanism, the OFP-TRM regulon could further our understanding of the developmental morphogenesis of tomato floral organs, serving as a gateway to generating beneficial alleles in agriculturally important crop species. Most *TRMs* that were previously described to function in regulating organ shapes of crops belong to *TRM* subclade I/*AtTRM1-5* (Wu *et al.*, 2018). The WT function of these *TRMs* is to elongate the organ in the proximal–distal direction and to reduce the width in the medial–lateral direction resulting in a narrow shape. This is demonstrated by *trm1-5* class mutants that have shorter, flatter, and wider organs (Lee *et al.*, 2006; S. Wang *et al.*, 2015; Zhou *et al.*, 2015; Wu *et al.*, 2018; Wang *et al.*, 2019). Surprisingly, the unknown role of the *TRMs* from subclade II, especially *SITRM17/20a* and *SITRM19*, was shown to reduce fruit elongation since the KO mutants showed an elongated tomato fruit shape. Furthermore,

the combination of *trm* mutants from these two clades appears to counter each other in fruit elongation, supporting a genetic interaction between these *TRMs*. Therefore, even within one regulon, OFP-TRM, the organ shape outcomes appear contradictory and imply multiple mechanisms that together ensure the appropriate morphology of plant organs.

We hypothesized that *TRMs* are involved in regulating cell division patterns as has been implied for *SITRM5*. Indeed, *TRM19* and *TRM17/20a* are also impacting cell division patterns but in an opposite manner than *SITRM5*. Interestingly, the extent of changing cell division patterning by *SITRM*s is dependent on the genetic background: whereas WT shows no or limited changes in cell division patterns or only in the medial–lateral direction, in the *o/s* background, cell division patterns are changed in the proximal–distal direction. In sum, *TRMs* appear to function in changing cell division patterns but not along one specific axis. The reason may lie in the notion that subclade I *TRM* proteins carry all eight domains, whereas the subclade II *TRM* proteins lack the M5 domain, which is of unknown function. Perhaps, this domain confers association with proteins that affect cell division planes. Additionally, subclade I *TRMs* typically carry only one M8 domain, whereas subclade II *TRMs* carry two M8 domains (Wu *et al.*, 2018). Since M8 is critical to the TRM-OFP interaction, additional M8 domains may cause a different interaction with the same *OFPs* or with two *OFPs* simultaneously. One *OFP* is thought to interact with *TRM* if the *TRM* has only one M8 domain. Thus, it is possible that two M8 domains interact with multiple *OFPs* resulting in different organ-shape outcomes. On the contrary, *TRMs* are not likely to directly impact the plane of cell division. If so, the effect on cell division for each gene can have opposing outcomes as is demonstrated by the phenotypes of the *Sltrm5* and *Sltrm19* mutants.

To investigate whether the relocalization of *SITRM5* to the cytosol when co-expressed with *OVATE* results in microtubule destabilization, we expressed MAP4, a microtubule-binding protein, together with *OVATE* and *SITRM5* in *N. benthamiana* epidermal cells. The results showed that *SITRM5* relocalization was not due to destabilization, suggesting that OFP-TRM interaction does not affect microtubule integrity (Fig. S6). Previously, we showed that oryzalin treatment disrupted the microtubular association of MAP4, *TRM5*, and *SITRM3/4* (Wu *et al.*, 2018) implying that these proteins assemble at this subcellular compartment.

To further understand the role of the TRM-OFP regulon in the control of fruit shape, we sought to test the interaction of *OVATE* and *SIOFP20* with the M8 domain in the *TRMs* in *planta*. Based on the subcellular localization patterns of co-expressed proteins in tobacco leaf epidermal cells, the M8 domain is critical for the TRM-OFP interaction. The M8 mutations that were generated in *planta* for *SITRM5* and *SITRM3/4* showed a strong reduction in colocalization when expressed in tobacco leaf epidermal cells. However, the effect of these mutations on fruit shape was less clear. The *SITRM3/4*^{M8} and *SITRM5*^{M8} alleles slightly enhanced elongated shape in the *o/s* background, while no effect of these mutations was found in the WT background. We hypothesized that shape would be altered

specifically in the WT background and to a more elongated shape. Considering that reduction or elimination of OVATE and SIOFP20 leads to elongated fruit shape by allowing SITRM5 and SITRM3/4 to remain on the MT and thereby increasing fruit elongation concomitantly with reducing fruit widening. Conversely, elimination of SITRM5 and SITRM3/4 leads to a reduction in fruit elongation by OVATE and SIOFP20 activity that is no longer countered by the TRMs. If so, we would expect that abolishing the interaction between OVATE and SIOFP20 and SITRM5^{M8} and SITRM3/4^{M8} permits the TRMs to remain on the microtubules and thereby enhancing fruit elongation. The slightly enhanced fruit shape in *ols/t3^{M8}/t5^{M8}* may be a consequence of this notion but of OFP redundancy as well. The reduced interactions of OFP and SITRM5^{M8} and SITRM3/4^{M8} in *N. benthamiana* could also suggest that functional interactions remain for SITRM5^{M8} *in planta*. The lack of a strong effect of the M8 mutants in the WT background may suggest that the TRM-OFP regulon contains other proteins to form a functional complex, consisting for example of the other components of the TTP complex. The larger multiprotein complex may not be affected greatly by mutations in the M8 domain of SITRM5 and SITRM3/4. Although these data do not clearly elucidate the role of the M8 domain *in planta*, they suggest that the relocalization of protein complexes seen in *N. benthamiana* may have a more complex role in regulating fruit shape than initially hypothesized (Wu *et al.*, 2018).

For the co-expression analyses, the GO terms of particular interest were those associated with cell division, cell cycle progression, cell wall organization, and microtubules. This is because the effect on fruit shape in *ols*, and *t3* and *t5* were associated with cell division patterning. Moreover, co-expression analyses in tobacco leaf cells show the association of TRMs with the cytoskeleton. GO terms related to cell division were shared in the SITRM5 and SITRM19/SITRM26a clusters. Interestingly, *Sltrm5* and *Sltrm19* mutants alone had the most distinct effect on fruit shape. This suggests that the enrichment for co-expressed genes involved in cell cycle progression in conjunction with cytoskeleton organization may represent important aspects of the molecular mechanism that is regulated by these two TRMs. Moreover, the results suggest that the cell cycle progression and cytoskeleton organization impact organ shape in both proximal–distal and mediolateral directions as the *Sltrm5* and *Sltrm19* mutants have opposing phenotypes. Other than tomato, the roles of the TRMs have been investigated primarily in *Arabidopsis*. *Attrm6l7/8* mutants do not produce the PPB, a microtubular structure that highlights the position of the future phragmoplast. The mis-regulation of the PPB impacts the orientation of cell divisions (Schaefer *et al.*, 2017). Another TRM, *AtTRM4*, is involved in the organization of cortical microtubules and the orientation of cellulose microfibrils potentially through direct interaction with Cellulose Synthase 3 (Yang *et al.*, 2019). Interestingly, *SITRM3/4* is the highest expressed in developing seeds similar to its possible ortholog *AtTRM4* in *Arabidopsis*. This suggests that SITRM3/4 could impact cortical microtubules and its interaction with cellulose synthase 3 in tomato as well. Ultimately, the co-expression analyses in combination with the genetic interactions suggest that

the interactions between OFPs and TRMs may involve multiple and partially redundant TRM-OFP pairings to regulate the shape of organs as they emerge and then enlarge during development. Furthermore, the modularity of the TRM-OFP pairings may be an underlying mechanism for generating species-specific modifications of corresponding organ shapes throughout plant species.

Acknowledgements

This project was funded through the AFRI grant 2017-67013-26199 of the USDA NIFA, NSF IOS 2048425 to EK, and the AFRI Postdoctoral Fellowship 2019-67012-29596 of the USDA NIFA to AS. We acknowledge the collaboration with the Biomedical Microscopy Core at the University of Georgia in the production of the confocal images in this paper.

Competing interests

None declared.

Author contributions

BZ and EK designed the research. BZ, QL, NK, NT, and MS performed the experiments. BZ analyzed the phenotypic and cellular data. BZ, NT, MS, and AS conducted the gene expression analysis. BZ, AS, and EK wrote the paper. BZ, QL, and NK contributed equally to this work.

ORCID

Neda Keyhaninejad  <https://orcid.org/0009-0007-7966-5046>

Esther van der Knaap  <https://orcid.org/0000-0003-4963-7427>

Qiang Li  <https://orcid.org/0000-0002-1686-9005>

Manoj Sapkota  <https://orcid.org/0000-0002-9987-1193>

Nathan Taitano  <https://orcid.org/0000-0002-0437-1584>

Biyao Zhang  <https://orcid.org/0009-0007-0373-8720>

Data availability

The data that support the findings of this study are available from the corresponding author upon reasonable request.

References

- Abramoff MD, Magalhães PJ, Ram SJ. 2004. Image processing with IMAGEJ. *Biophotonics International* 11: 36–42.
- Alexa A, Rahnenfuhrer J. 2021. *TOPGO: enrichment analysis for gene ontology*. R package v.2.44.0. [WWW document] URL <https://bioconductor.org/packages/topGO/> [accessed 13 March 2023].
- Azimzadeh J, Nacry P, Christodoulidou A, Drevensek S, Camilleri C, Amieur N, Parcy F, Pastuglia M, Bouchez D. 2008. Arabidopsis TONNEAU1 proteins are essential for preprophase band formation and interact with centrin. *Plant Cell* 20: 2146–2159.
- Borovsky Y, Raz A, Doron-Faigenboim A, Zemach H, Karavani E, Paran I. 2021. Pepper fruit elongation is controlled by *Capsicum annuum* ovate family protein 20. *Frontiers in Plant Science* 12: 815589.

- Drevensek S, Goussot M, Duroc Y, Christodoulidou A, Steyaert S, Schaefer E, Duvernois E, Grandjean O, Vantard M, Bouchez D *et al.* 2012. The Arabidopsis TRM1-TON1 interaction reveals a recruitment network common to plant cortical microtubule arrays and eukaryotic centrosomes. *Plant Cell* 24: 178–191.
- Kim D, Paggi JM, Park C, Bennett C, Salzberg SL. 2019. Graph-based genome alignment and genotyping with HISAT2 and HISAT-genotype. *Nature Biotechnology* 37: 907–915.
- Langfelder P, Horvath S. 2008. WGCNA: an R package for weighted correlation network analysis. *BMC Bioinformatics* 9: 559.
- Lazzaro MD, Wu S, Snouffer A, Wang Y, van der Knaap E. 2018. Plant organ shapes are regulated by protein interactions and associations with microtubules. *Frontiers in Plant Science* 9: 1766.
- Lee YK, Kim GT, Kim IJ, Park J, Kwak SS, Choi G, Chung WI. 2006. *LONGIFOLIA1* and *LONGIFOLIA2*, two homologous genes, regulate longitudinal cell elongation in Arabidopsis. *Development* 133: 4305–4314.
- Liu J, Van Eck J, Cong B, Tanksley SD. 2002. A new class of regulatory genes underlying the cause of pear-shaped tomato fruit. *Proceedings of the National Academy of Sciences, USA* 99: 13302–13306.
- Rasmussen CG, Bellinger M. 2018. An overview of plant division-plane orientation. *New Phytologist* 219: 505–512.
- Rodriguez GR, Kim HJ, van der Knaap E. 2013. Mapping of two suppressors of *OVATE* (*sov*) loci in tomato. *Heredity* 111: 256–264.
- Rodriguez GR, Moysenko JB, Robbins MD, Morejon NH, Francis DM, van der Knaap E. 2010. TOMATO ANALYZER: a useful software application to collect accurate and detailed morphological and colorimetric data from two-dimensional objects. *Journal of Visualized Experiments* 37: 1856.
- Schaefer E, Belcram K, Uytewaal M, Duroc Y, Goussot M, Legland D, Laruelle E, de Tauzia-Moreau ML, Pastuglia M, Bouchez D. 2017. The preprophase band of microtubules controls the robustness of division orientation in plants. *Science* 356: 186–189.
- Schmitz AJ, Begcy K, Sarath G, Walia H. 2015. Rice Ovate Family Protein 2 (OFP2) alters hormonal homeostasis and vasculature development. *Plant Science* 241: 177–188.
- Serin EA, Nijveen H, Hilhorst HW, Ligterink W. 2016. Learning from co-expression networks: possibilities and challenges. *Frontiers in Plant Science* 7: 444.
- Sherley JL, Stadler PB, Stadler JS. 1995. A quantitative method for the analysis of mammalian cell proliferation in culture in terms of dividing and non-dividing cells. *Cell Proliferation* 28: 137–144.
- Snouffer A, Kraus C, van der Knaap E. 2020. The shape of things to come: ovate family proteins regulate plant organ shape. *Current Opinion in Plant Biology* 53: 98–105.
- Spinner L, Gadeyne A, Belcram K, Goussot M, Moison M, Duroc Y, Eeckhout D, De Winne N, Schaefer E, Van De Slijke E *et al.* 2013. A protein phosphatase 2A complex spatially controls plant cell division. *Nature Communications* 4: 1863.
- Stuart JM, Segal E, Koller D, Kim SK. 2003. A gene-coexpression network for global discovery of conserved genetic modules. *Science* 302: 249–255.
- Supek F, Bosnjak M, Skunca N, Smuc T. 2011. REVIGO summarizes and visualizes long lists of gene ontology terms. *PLoS ONE* 6: e21800.
- Van Der Knaap E, Lippman ZB, Tanksley SD. 2002. Extremely elongated tomato fruit controlled by four quantitative trait loci with epistatic interactions. *Theoretical and Applied Genetics* 104: 241–247.
- Wang S, Chang Y, Guo J, Chen JG. 2007. Arabidopsis Ovate Family Protein 1 is a transcriptional repressor that suppresses cell elongation. *The Plant Journal* 50: 858–872.
- Wang S, Chang Y, Guo J, Zeng Q, Ellis BE, Chen JG. 2011. Arabidopsis ovate family proteins, a novel transcriptional repressor family, control multiple aspects of plant growth and development. *PLoS ONE* 6: e23896.
- Wang S, Li S, Liu Q, Wu K, Zhang J, Wang S, Wang Y, Chen X, Zhang Y, Gao C *et al.* 2015. The OsSPL16-GW7 regulatory module determines grain shape and simultaneously improves rice yield and grain quality. *Nature Genetics* 47: 949–954.
- Wang W, Pan Q, Tian B, He F, Chen Y, Bai G, Akhunova A, Trick HN, Akhunov E. 2019. Gene editing of the wheat homologs of *TONNEAU1* recruiting motif encoding gene affects grain shape and weight in wheat. *The Plant Journal* 100: 251–264.
- Wang Y, Xiong G, Hu J, Jiang L, Yu H, Xu J, Fang Y, Zeng L, Xu E, Xu J *et al.* 2015. Copy number variation at the *GL7* locus contributes to grain size diversity in rice. *Nature Genetics* 47: 944–948.
- Wickham H. 2011. GGLOT2. *Wiley Interdisciplinary Reviews: Computational Statistics* 3: 180–185.
- Wu S, Clevenger JP, Sun L, Visa S, Kamiya Y, Jikumaru Y, Blakeslee J, van der Knaap E. 2015. The control of tomato fruit elongation orchestrated by sun, ovate and fs8.1 in a wild relative of tomato. *Plant Science* 238: 95–104.
- Wu S, Zhang B, Keyhaninejad N, Rodriguez GR, Kim HJ, Chakrabarti M, Illa-Berenguer E, Taitano NK, Gonzalo MJ, Diaz A *et al.* 2018. A common genetic mechanism underlies morphological diversity in fruits and other plant organs. *Nature Communications* 9: 4734.
- Yang B, Voiniciuc C, Fu L, Dieluwit S, Klose H, Usadel B. 2019. TRM4 is essential for cellulose deposition in Arabidopsis seed mucilage by maintaining cortical microtubule organization and interacting with CESA3. *New Phytologist* 221: 881–895.
- Yang C, Ma Y, He Y, Tian Z, Li J. 2018. OsOFP19 modulates plant architecture by integrating the cell division pattern and brassinosteroid signaling. *The Plant Journal* 93: 489–501.
- Yang C, Shen W, He Y, Tian Z, Li J. 2016. OVATE Family Protein 8 positively mediates brassinosteroid signaling through interacting with the GSK3-like kinase in rice. *PLoS Genetics* 12: e1006118.
- Zhang X, Wu J, Yu Q, Liu R, Wang ZY, Sun Y. 2020. AtOFPs regulate cell elongation by modulating microtubule orientation via direct interaction with TONNEAU2. *Plant Science* 292: 110405.
- Zhao DS, Li QF, Zhang CQ, Zhang C, Yang QQ, Pan LX, Ren XY, Lu J, Gu MH, Liu QQ. 2018. GS9 acts as a transcriptional activator to regulate rice grain shape and appearance quality. *Nature Communications* 9: 1240.
- Zhou Y, Miao J, Gu H, Peng X, Leburu M, Yuan F, Gu H, Gao Y, Tao Y, Zhu J *et al.* 2015. Natural variations in *SLG7* regulate grain shape in rice. *Genetics* 201: 1591–1599.

Supporting Information

Additional Supporting Information may be found online in the Supporting Information section at the end of the article.

Fig. S1 Expression patterns of *OVATE*, *S/OFP20*, and selected *S/ITRMs*.

Fig. S2 Mutant alleles of five TONNEAU1 Recruiting Motif proteins created by CRISPR/Cas9 genome editing.

Fig. S3 Rescuing fruit shape of *ovate1 Slofp20 (ols)* by *Sltrm3/4-2 (t3)* and *Sltrm5-2 (t5)*.

Fig. S4 Shape indices of vegetative and floral organs in *trms* in the wild-type and *ovate1 Slofp20* background.

Fig. S5 Colocalization of wild-type and M8 domain mutants of *OVATE* and TONNEAU1 Recruiting Motif proteins in *Nicotiana benthamiana* leaf epidermal cells.

Fig. S6 Co-expression of *S/ITRM5* and *OVATE* does not lead to depolymerization of microtubules.

Fig. S7 Three additional biological replicates showing the phenotype of M8 domain mutants *in planta*.

Fig. S8 Synergistic interactions between *Slrm17/20a* and *Slrm19*.

Fig. S9 Contrasting phenotype of *t5-2* and *t19-2* in wild-type background.

Fig. S10 Ovary shape at anthesis in *ovate (o)*, *SIOFP20 (s)*, and mutants in the two TONNEAU1 Recruiting Motif protein subclades.

Fig. S11 Cell shape index in the proximal end area of all genotypes.

Table S1 Primers used in the study on tomato (*Solanum pimpinellifolium*) fruit shape.

Table S2 Curated GO terms enriched in co-expression cluster for WGCNA co-expression networks.

Please note: Wiley is not responsible for the content or functionality of any Supporting Information supplied by the authors. Any queries (other than missing material) should be directed to the *New Phytologist* Central Office.